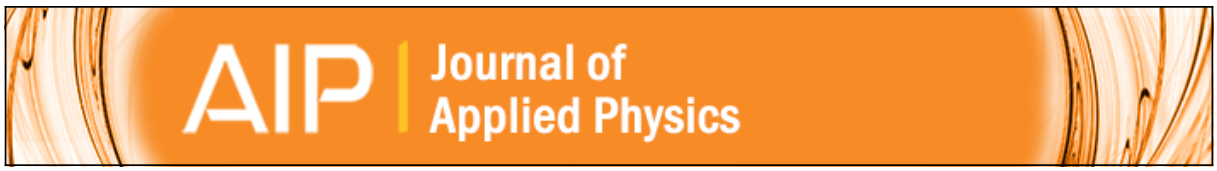

Local structure change evidenced by temperature-dependent elastic measurements: Case study on Bi1/2Na1/2TiO3-based lead-free relaxor piezoceramics

Robert Dittmer, Wook Jo, Kyle G. Webber, Jacob L. Jones, and Jürgen Rödel

Citation: Journal of Applied Physics **115**, 084108 (2014); doi: 10.1063/1.4866092

View online: http://dx.doi.org/10.1063/1.4866092

View Table of Contents: http://scitation.aip.org/content/aip/journal/jap/115/8?ver=pdfcov

Published by the AIP Publishing

Local structure change evidenced by temperature-dependent elastic measurements: Case study on $Bi_{1/2}Na_{1/2}TiO_3$-based lead-free relaxor piezoceramics

Robert Dittmer,[1] Wook Jo,[1,a)] Kyle G. Webber,[1] Jacob L. Jones,[2] and Jürgen Rödel[1]
[1]*Institute of Materials Science, Technische Universität Darmstadt, Alarich-Weiss-Str. 2, 64287 Darmstadt, Germany*
[2]*Materials Science and Engineering, University of Florida, 135A Rhines Hall, Gainesville, Florida 32611-6400, USA*

(Received 11 December 2013; accepted 5 February 2014; published online 26 February 2014)

The temperature-dependent Young's modulus $Y(T)$ of the lead-free piezoceramics of $0.8Bi_{1/2}Na_{1/2}TiO_3$-$0.2Bi_{1/2}K_{1/2}TiO_3$ (20BKT) and $0.96(0.8Bi_{1/2}Na_{1/2}TiO_3$-$0.2Bi_{1/2}K_{1/2}TiO_3)$-$0.04$ $BiZn_{1/2}Ti_{1/2}O_3$ (4BZT) is measured with the impulse excitation technique and contrasted with corresponding dielectric and structural data. While the dielectric properties suggest a phase transition, the high resolution XRD patterns remain virtually unchanged from room temperature up to high temperatures, confirming no change in their long-range order. In contrast, the elastic properties indicate a broad and diffuse ferroelastic transition denoted by a minimum in $Y(T)$. By analogy to the elastic and dielectric data of $PbZr_xTi_{1-x}O_3$ and PLZT, it is concluded that 20BKT and 4BZT are relaxors with polar nanoregions embedded in a metrically cubic matrix. Interestingly, no indication for the freezing temperature was reflected in any of the employed measurement techniques. From the saturation of $Y(T)$, it is suggested that the Burns temperature may be approximated as 700 °C. Moreover, it is found that the modification with the ternary end-member $BiZn_{1/2}Ti_{1/2}O_3$ results in an increase in Young's modulus. A comparison with the $Bi_{1/2}Na_{1/2}TiO_3$-$BaTiO_3$-$K_{0.5}Na_{0.5}NbO_3$ yields the same results. © *2014 AIP Publishing LLC*. [http://dx.doi.org/10.1063/1.4866092]

I. INTRODUCTION

Piezoceramics based on bismuth sodium titanate[1] $Bi_{1/2}Na_{1/2}TiO_3$ (BNT) have attracted considerable attention in the search for lead-free alternatives to the ubiquitous lead zirconate titanate $PbZr_xTi_{1-x}O_3$ (PZT).[2,3] Pseudobinary solid solutions with $BaTiO_3$ (BT) or $Bi_{1/2}K_{1/2}TiO_3$ (BKT) were shown to exhibit peculiar features like a field-induced phase transition[4,5] and a frequency-dispersive local maximum in the temperature-dependent permittivity.[6,7] Chemical modifications afford to tailor the properties for specific applications. For example, incorporation of $K_{0.5}Na_{0.5}NbO_3$ (KNN),[8] $SrTiO_3$ (ST),[9] $BiAlO_3$ (BA),[10] or $BiZn_{1/2}Ti_{1/2}O_3$ (BZT)[11] allows for large field-induced strains, the origin of which was recently identified as incipient piezoelectricity,[12,13] or nearly temperature-insensitive permittivity for high-temperature capacitors.[14]

The crystal structure and its thermal evolution are still under debate for many BNT-based systems.[3,15] High-temperature diffraction studies have so far not provided a conclusive explanation for the features observed in the high-temperature permittivity measurements possibly due to the inherent resolution limit of the diffraction techniques.[16] In other words, the entities responsible for the observed electrical properties, e.g., polar nanoregions (PNRs) are too small to be resolved by conventional diffraction techniques. BNT-based materials have been suggested to be relaxor ferroelectrics that feature PNRs embedded in a metrically cubic phase.[17,18] With sizes typically below 10 nm, these PNRs fall below the correlation length of X-ray and neutron diffraction experiments, and are, therefore, hard to detect. Consequently, the diffraction patterns appear metrically cubic with a strongly diffuse background.

Measurement of the temperature-dependent elastic properties provides a powerful tool to monitor temperature-driven processes. Hence, it offers a natural pathway to detect phase transitions as $Y(T)$ depends on the interatomic or ionic bonding strength. For example, the sequence of three phase transitions in barium titanate is clearly reflected in changes of the Young's modulus.[19] At the paraelectric (PE) to ferroelectric (FE) transition at ~130 °C, the Young's modulus decreases by almost 50% within a very narrow temperature range. Bourim *et al.*[20,21] observed that the sharp change in the shear modulus of the first order PE-FE transition in PZT is associated with a sharp maximum in internal friction. This energy dissipation was rationalized with the motion of domain walls, which is suggested to be viscous in nature and affects not only the mechanical losses but also dielectric losses.[22] Later, a slightly revised phase diagram for PZT was proposed based on low temperature measurements of elastic moduli.[23] For the canonical relaxor PMN, it was demonstrated that the frequency-dispersive broad maximum in permittivity is correlated with a minimum in elastic stiffness and a subsequent saturation.[24] The likewise canonical relaxor PLZT 8/65/35 reveals a similar minimum in $Y(T)$, however, well below the maximum in the dielectric permittivity.[25]

a)Author to whom correspondence should be addressed. Electronic mail: jo@ceramics.tu-darmstadt.de

Consequently, it is appealing to employ elastic measurements to clarify the underlying physical mechanisms for the peculiar dielectric properties of lead-free BNT-based relaxors. Unfortunately, little is known about the elastic behavior of these materials. For the presumably morphotropic phase boundary (MPB) composition BNT-6BT Cordero *et al.*[26] observed a maximum in the compliance at approximately 190 °C, which was confirmed by other authors.[27] The relaxor features of BNT-6BT, however, were not reflected in their analysis, since BNT-6BT at the time was predominantly assumed to be a ferroelectric transforming into an antiferroelectric before it converts into a paraelectric cubic phase.[7] Moreover, the study was limited to the pseudobinary BNT-100xBT systems. It is currently not known whether a ternary end-member like BZT or KNN, which are known to have tremendous effects on the constitutive large and small signal behavior, has a significant effect on the elastic properties.

In this work, we use the impulse excitation technique to investigate the temperature-dependent Young's modulus for two unpoled lead-free compositions: BNT-20BKT and BNT-20BKT-4BZT. The former represents a nonergodic relaxor while the latter embodies an ergodic relaxor. The dielectric response was measured for various frequencies and compared with the elastic behavior. In order to thoroughly discuss the structure-property relationship, temperature-dependent high-energy X-ray diffraction measurements were performed. To resolve the expected minute changes in symmetry, a high resolution detector was employed that features a maximum resolution $\Delta Q \cdot Q^{-1}$ of up to 2×10^{-4}.

II. EXPERIMENTAL

A. Sample preparation

Within this work the primarily investigated compositions are $0.8Bi_{1/2}Na_{1/2}TiO_3$-$0.2Bi_{1/2}K_{1/2}TiO_3$ and $0.96(0.8Bi_{1/2}Na_{1/2}TiO_3$-$0.2Bi_{1/2}K_{1/2}TiO_3)$-$0.04BiZn_{1/2}Ti_{1/2}O_3$, referred to as BNT-20BKT and BNT-20BKT-4BZT, respectively. As reference, commercially available soft ferroelectric PZT PIC151 (PI ceramics, Lederhose, Germany) and relaxor PLZT 8/65/35 (Boston Applied Technologies, Inc., Wobum, MA, USA) were also characterized. Polycrystalline $0.94Bi_{1/2}Na_{1/2}TiO_3$-$0.06BaTiO_3$ (BNT-6BT) and $0.98(0.94Bi_{1/2}Na_{1/2}TiO_3$-$0.06BaTiO_3)$-$0.02K_{0.5}Na_{0.5}NbO_3$ (BNT-6BT-2KNN) were synthesized by means of a mixed oxide route. The raw powders (all Alfa Aesar GmbH, Karlsruhe, Germany) Bi_2O_3 (99.975% purity), Na_2CO_3 (99.5%), $BaCO_3$ (99.8%), K_2CO_3 (99.0%), ZnO_2 (99.99%), Nb_2O_5 (99.9%), and TiO_2 (99.9%) were weighed according to the respective stoichiometric formula using a precision balance (TE214S, Sartorius AG, Göttingen, Germany). Subsequent mixing was performed in a planetary mill (Pulverisette 5, Fritsch GmbH, Idar-Oberstein, Germany) with custom-made polyamide containers and zirconia milling balls (Mühlheimer GmbH, Bärnau, Germany). The milling was done for 24 h at 250 rpm using ethanol as milling medium. The slurries were subsequently dried in an oven (Memmert GmbH + Co. KG, Schwabach, Germany) at 100 °C. After pestling, the powders were calcined in covered alumina crucibles using a box furnace (L9/KM, Nabertherm GmbH, Lilienthal, Germany) with a dwell time of 3 h at temperatures of 900 °C. After another milling and drying step, the powders were manually pressed in a custom-made steel die. The dielectric measurements were conducted on disc-shaped samples made from a die with a 10 mm diameter. Bar-type samples for elastic measurements were shaped by a die with a 4×40 mm^2 cavity. In the next step, the samples were pressed cold-isostatically (KIP 100 E, Paul-Otto Weber GmbH, Remshalden, Germany) and then sintered in covered alumina crucibles for 3 h at 1150 °C with a heating rate of 5 °C/min in a box furnace (L16/14, Nabertherm GmbH, Lilienthal, Germany). In order to minimize the evaporation of volatile elements, the samples were partially covered in powder of the respective composition. By subsequent grinding, the sample geometry was adjusted and a surface layer of at least 200 μm was removed. Specimens for elastic measurements had a size of approximately $3 \times 3 \times 35$ mm^3, while specimens for dielectric measurements had a diameter of 7 mm and a height of 0.7 mm.

B. Dynamic Young's modulus

The measurement of the fundamental flexural resonance frequency f_R was performed on unpoled bar-type samples with a cross-sectional area of 3×3 mm^2 at a resonance frequency using a damping analyzer (RFDA-HT1750, IMCE, Genk, Belgium). This technique, referred to as the impulse excitation technique, acoustically measures the natural frequency of the sample in response to a small mechanical impulse. The Young's modulus Y was calculated from the resonance frequency f_R by means of the following equation:[28]

$$Y(f_R) = 0.9465 \cdot \left(\frac{m \cdot f_R^2}{b}\right) \cdot \left(\frac{L^3}{t^3}\right) \cdot T_l, \tag{1}$$

where mass m, width b, length L, thickness t, and a correction factor T_l that accounts for the finite thickness of the bar and the Poisson's ratio. Since the Poisson's ratio is not known, the following approximation is applied:[29]

$$T_l = 1 + 6.575 \cdot \left(\frac{t}{L}\right)^2. \tag{2}$$

In contrast to macroscopically piezoelectric specimens, the Young's modulus of unpoled materials does not depend on whether the electrodes are short-circuited or open. The resonance frequency is recorded for both heating and cooling with a maximum temperature of 700 °C and a heating and cooling rate of 2 K·min^{-1}.

C. Dielectric measurements

The temperature-dependent dielectric behavior of unpoled specimens was measured with an impedance analyzer (HP4284A, Hewlett Packard Japan, LTD., Kobe, Japan). The custom-built sample holder consisted of a platinum top and bottom electrode and was placed into a box furnace (LE4/11/R6, Nabertherm GmbH, Lilienthal, Germany). Using a ramp of 2 K·min^{-1}, the permittivity was measured for temperatures up to 400 °C at the frequencies of 0.1 kHz,

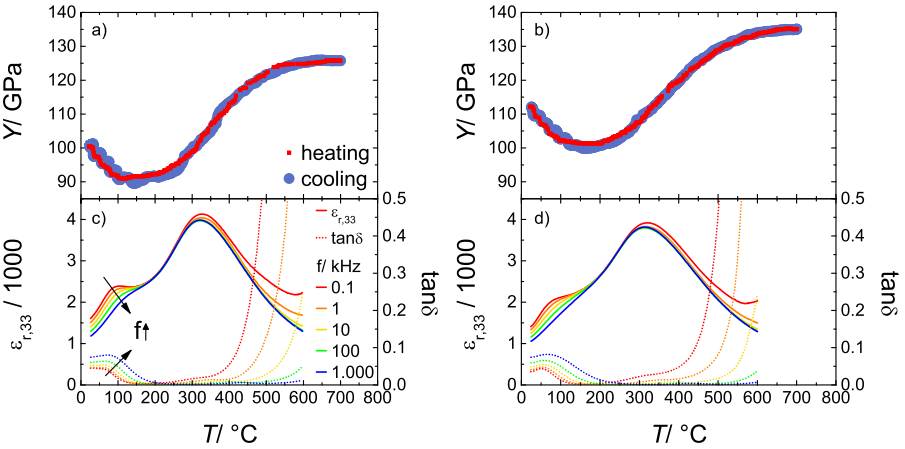

FIG. 1. Young's modulus and dielectric properties for (a) and (c) BNT-20BKT and (b) and (d) BNT-20BKT-4BZT (b) and (d).

1 kHz, 10 kHz, 100 kHz, and 1000 kHz with a measurement amplitude of 1 V. A LabVIEW program was used for data-acquisition by means of an analog-digital-converter (TI GPIB-USB-HS, Texas Instruments, Inc., Dallas, TX, USA).

D. High-temperature X-ray diffraction

The high-temperature XRD measurements were performed at the 11BM-B beamline at the Advanced Photon Source (APS) within the Argonne National Laboratory (Lemont, IL, USA). Disc-shaped ceramic samples of compositions BNT-20BKT and BNT-20BKT-4BZT were ground using a mortar and pestle and annealed for 30 min at 400 °C. The powder was loosely filled into a quartz capillary with a diameter of 0.7 mm, which was then mounted into a goniometer head for alignment and spun with >90 Hz. Placed into the high-energy, monochromatic X-ray beam with a wavelength of 0.0458739 nm, the diffraction patterns were collected from $0.5° < 2\theta < 38°$. The detector is a multi-analyzer array consisting of 12 independent Si(111) crystal analyzers and $LaCl_3$ scintillation detectors allowing for high resolutions of approximately $\Delta Q/Q \approx 2 \times 10^{-4}$ with Q being the scattering angle. Temperature control was realized by means of a hot gas blower (Cyberstar, Echirolles, France). Diffraction patterns with a collection time of 2 min were recorded consecutively during increasing temperature with a heating ramp of 5 K·min^{-1} to 350 °C. The step width was $\theta = 0.002°$.

III. RESULTS

The dynamic Young's modulus Y is presented in Fig. 1 as a function of temperature for unpoled BNT-20BKT and BNT-20BKT-4BZT. Both compositions show a strongly nonlinear temperature-dependent Young's modulus. At room temperature BNT-20BKT exhibits a Y of 100 GPa, decreasing upon heating down to a minimum of 91 GPa in the range of 100 °C–200 °C. Higher temperatures cause a stiffening of the sample; the Young's modulus increases and eventually shows a saturation behavior at approximately 127 GPa at 700 °C. BNT-20BKT-4BZT demonstrates the same behavior yet with a slightly higher Y at both room temperature (112 GPa) and 700 °C (135 GPa) with a minimum of 101 GPa. There is virtually no difference in the heating and the cooling curve of both compositions, that is, there is no apparent thermal hysteresis within the resolution of the measurements.

BNT-6BT and BNT-6BT-2KNN exhibit an equivalent thermal evolution of Y as demonstrated by Fig. 2. In addition, the unpoled lead-containing compounds PZT and PLZT likewise display a significant increase in Y. For PZT, the Young's modulus increases by 153% from 66 GPa at 25 °C to 167 GPa at 450 °C while for PLZT the Young's modulus increases by 67% from 98 GPa at room temperature to 164 GPa at 450 °C.

The dielectric response of both BNT-BKT-based materials displays two notable features. In a low-temperature

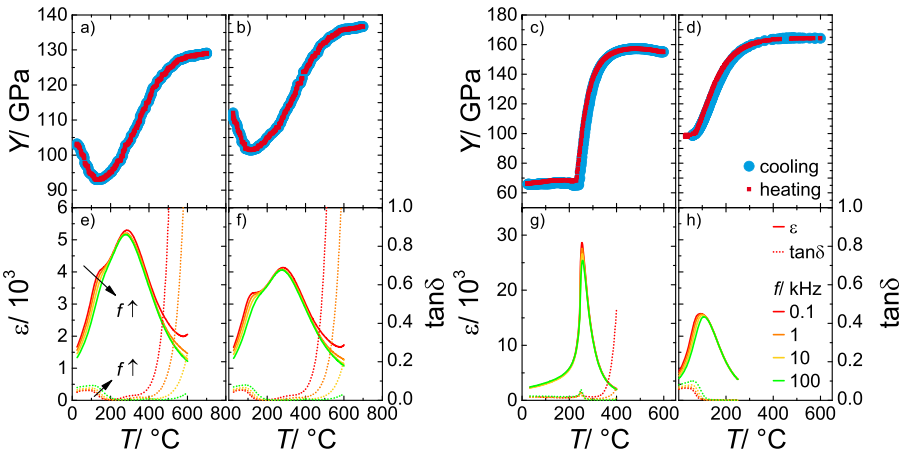

FIG. 2. Young's modulus in addition to permittivity and loss tangent for (a) and (e) BNT-6BT, (b) and (f) BNT-6BT-2KNN, (c) and (g) soft PZT, and (d) and (h) PLZT 8/65/35.

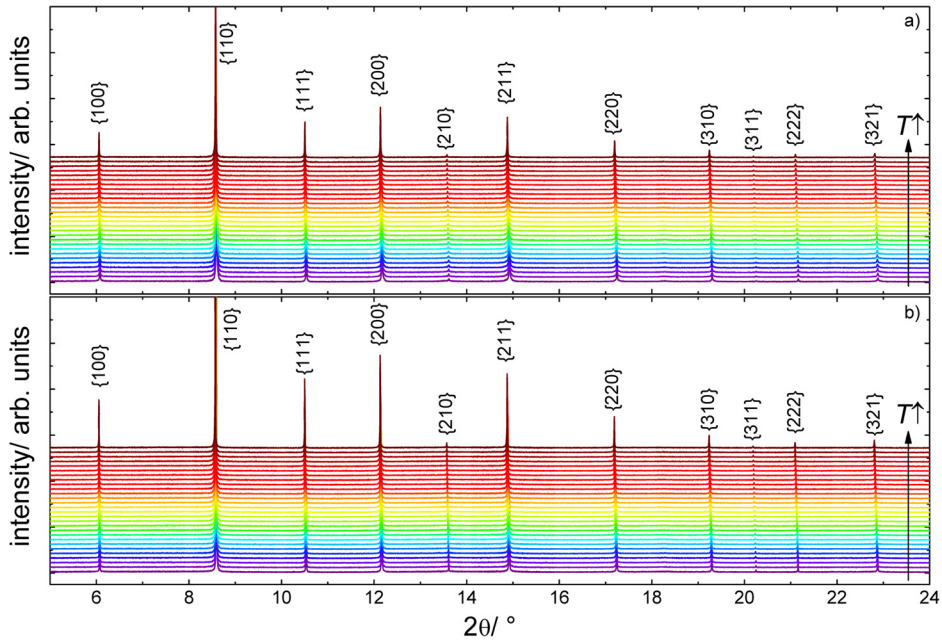

FIG. 3. Temperature-dependent diffraction patterns for (a) BNT-20BKT and (b) BNT-20BKT-4BZT from room temperature to 350 °C.

region up to approximately 200 °C, there is a frequency-dispersive shoulder in ε_r, i.e., higher frequencies cause a decrease in permittivity. The loss factor is likewise frequency-dependent as higher frequencies give rise to an increase in dielectric losses. This behavior is qualitatively the same for both compositions; however, the shoulder is slightly more pronounced for BNT-20BKT. At higher temperatures, the dispersion decreases and a maximum in $\varepsilon_r(T)$ emerges at a temperature $T_m = 327$ °C in BNT-20BKT and $T_m = 321$ °C in BNT-20BKT-4BZT. The corresponding peak permittivity at 100 Hz decreases by 5% from 4128 to 3917. Closer inspection reveals that this maximum also involves frequency dispersion, albeit minute, at the high-temperature side of the peak. Interestingly, a higher measurement frequency yields a higher permittivity and also higher losses, which is in contrast to the low-temperature shoulder where higher frequency f causes a decrease in $\tan\delta$.

Close inspection of the individual diffraction patterns at room temperature confirms a pseudocubic structure for both compositions (Fig. 3). Upon temperature increase, the shape of the reflections remains largely unchanged while shifting to lower 2θ values. This shift is caused by thermal expansion and visualized in detail for the $\{111\}_{pc}$ (where the subscript "pc" denotes pseudocubic indices) reflection in Fig. 4. The most striking difference between both compositions is the full width at half maximum (FWHM), which is notably higher for BNT-20BKT.

IV. DISCUSSION

The frequency dispersion observed in the dielectric measurements can be ascribed to the presence of PNRs and their dynamics.[17] The size distribution of these PNRs gives rise to a broad distribution of relaxation times. Thus, the measured permittivity depends on the probing frequency. At higher frequencies large, PNRs are too slow to follow the excitation field and, consequently, the permittivity decreases while the loss factor increases. In general, heating of a relaxor causes the shrinkage of PNRs.[17] The permittivity response increases because the "active" fraction of PNRs that may follow the external field increases. In the canonical lead-containing relaxors further heating reduces the overall volume fraction of PNRs; thus, the ε_r eventually peaks at a frequency-dependent temperature T_m beyond which the permittivity response declines. In BNT-based relaxors, however, the frequency dispersion almost vanishes approximately at 100 °C that is below the maximum permittivity.

In perovskites, a peak in permittivity often denotes a phase transition. In the case of the currently studied

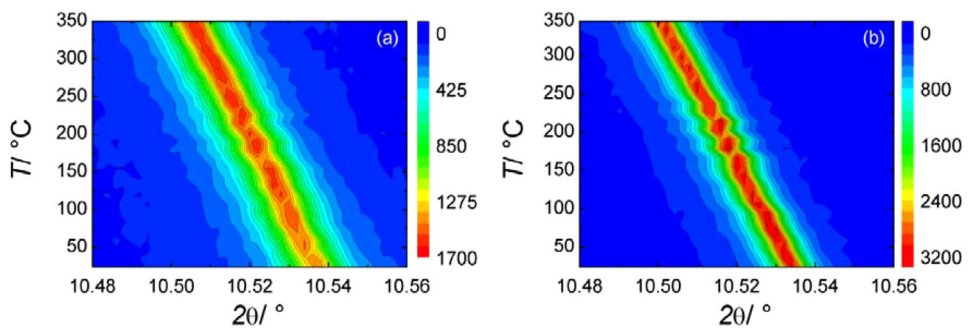

FIG. 4. Contour plot of the $\{111\}_{pc}$ reflection as a function of temperature for (a) BNT-20BKT and (b) BNT-20BKT-4BZT from room temperature up to 350 °C.

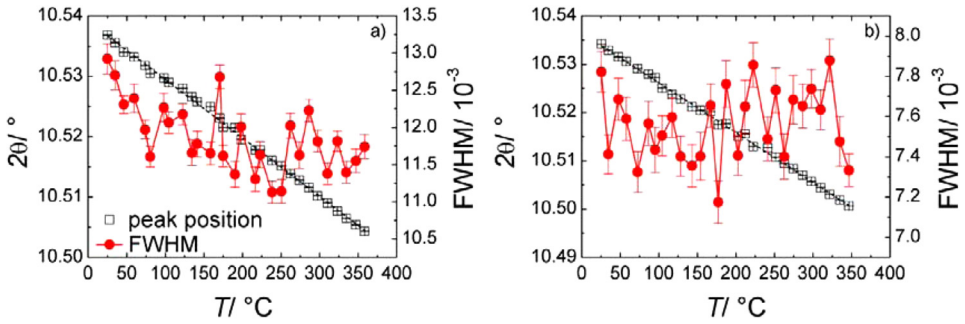

FIG. 5. Reflection angle 2θ and FWHM of the $\{111\}_{pc}$ reflection determined for (a) BNT-20BKT and (b) BNT-20BKT-4BZT from room temperature to 350 °C.

BNT-based ceramics, however, the diffraction patterns appear pseudocubic and there is no evidence for a temperature-driven phase transition. The observed changes can be attributed to thermal expansion. The $\{111\}_{pc}$ reflection was fit to a pseudo-Voigt function to determine the peak position and the FWHM as a function of temperature. According to Fig. 5, the coefficient of thermal expansion is very similar for both compositions. Linear fitting yields for the $\{111\}_{pc}$ reflection a shift of 9.7×10^{-5} K^{-1} for BNT-20BKT and 10.3×10^{-5} K^{-1} for BNT-20BKT-4BZT. The FWHM found for BNT-20BKT is 12×10^{-3} (deg.) for the $\{111\}_{pc}$ reflection compared to around 7.5×10^{-3} (deg.) for the corresponding reflection in BNT-20BKT-4BZT. Across the investigated temperature range, the FWHM of both compositions is nearly invariant. Therefore, the diffraction experiments do not reveal any symmetry breaking with increasing temperature. Structural phase transitions are typically observed when the symmetry decreases due to splitting in characteristics peaks, e.g., $\{111\}_{pc}$ in rhombohedral or $\{200\}_{pc}$ in tetragonal symmetry. In the present work, a subtle distortion that may be present at low temperature may be measured in a broader FWHM. If a phase transition occurs with increasing temperature, a decrease in the FWHM might be expected. In the present results, little change in FWHM was detected across the entire measured temperature range. Thus, it can be concluded that the effects contributing to the dielectric and elastic behaviors are of a length below the coherence length for X-ray diffraction. For example, the canonical relaxor PMN remains pseudocubic from −268 °C to 620 °C,[30] while similar results have been reported also for $Pb(Mg_{1/3}Ta_{2/3})O_3$.[31] In addition, high-temperature diffraction measurements reported for related lead-free BNT-based materials comply with the currently observed temperature invariance of the structure.[32–34]

In contrast to the XRD patterns, the Young's modulus changes significantly with temperature. In many ceramics, such as alumina[35] or magnesia,[36] the Young's modulus decreases linearly with temperature as long as structural phase transformations are absent. This observation is generally explained by the decreasing strength of bonds with temperature, that is, the slope of the asymmetric interatomic potential curve decreases with temperature.[37] It was proposed by Wachtman *et al.*[38] that the Young's modulus in oxides actually displays exponential temperature dependence in the form of

$$Y(T) = Y_{0K} - A \cdot T \cdot \exp(-T_0/T), \qquad (3)$$

where the Young's modulus Y_{0K} at absolute zero temperature and the constants T_0 and A. For high temperatures, the term $\exp(-T_0/T)$ approaches unity and, therefore, a linear dependence is observed at room temperature and beyond. A deviation from this general behavior is observed when a material undergoes structural changes such as phase transition,[39] glass transition,[40] or changes in the microstructure[41] due to the appearance or closure of microcracking or changes in grain boundary characteristics. Within the context of ferroelectric materials, a significant softening is expected when a paraelastic-to-ferroelastic transition takes place, which is usually at the Curie point T_c, due to the formation of ferroelastic domains.[42] It follows that an unusual softening leading to a negative deviation from the usual linear decrease with increasing temperature can happen when ferroelastic transition occurs. In the case of the ferroelastic transition, the Young's modulus is expected to establish a local minimum around the transition point due to the multiplication of equally stable orientations of coexisting symmetries.

The observed profiles of the temperature-dependent Young's modulus plot shown in Fig. 1 are untypical in that they show two distinctive anomalies. One is a diffuse local minimum in the temperature range at approximately 150 °C, and the other is an increase of Young's modulus asymptotically to a saturation behavior. By contrast, no such minimum is found in PZT. Instead, the Young's modulus is virtually constant up to about 230 °C and subsequently increases sharply with a maximum slope at 234 °C (Figure 2(c)). This abrupt change denotes a ferroelastic-to-paraelastic (or equivalently ferroelectric-to-paraelectric in this case) phase transition, which is also reflected in the dielectric constant peaking at about 250 °C. The same principle trend is reported not only for PZT[21] but also for Mn-doped PMN-PT,[43,44] where the FE-PE transition at 170 °C complies with a peak in permittivity.[43,44] As demonstrated by Fig. 6, the maximum in $\varepsilon(T)$ is shifted for PLZT as compared to PZT. In agreement with earlier reports,[45] not only the temperature of maximum permittivity T_m is lowered but also the transition spans a broader temperature range than in PZT.[46] This broadening effect was rationalized with the disruption of long-range order, i.e., the formation of PNRs and their reduction in size with increasing lanthanum content.[47] In other words, the conversion of ferroelastic PNRs into paraelastic cubic matrix takes place over a wide range of temperature. The temperature-dependent Young's modulus likewise reveals a broadening. This means that the relaxor nature is indeed reflected in the temperature-dependence of the Young's modulus.

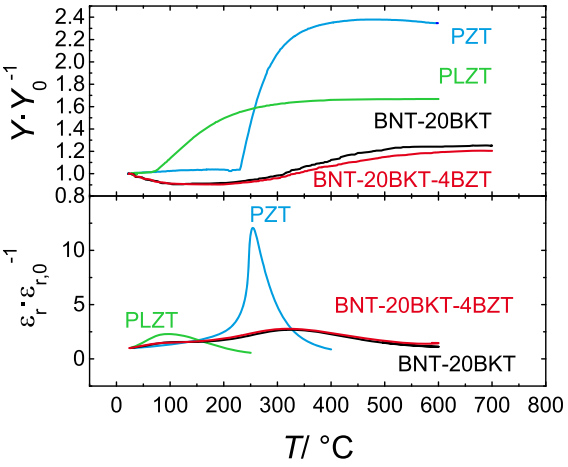

FIG. 6. Comparison of PLZT, PZT, 20BKT, and 4BZT in terms of resonance frequency and relative dielectric permittivity normalized to their respective room temperature value.

The comparison with PLZT suggests that the temperature dependent Young's modulus above 200 °C is due to a gradual conversion of ferroelastic PNRs into paraelastic cubic matrix, while the presence of a local minimum in the Young's modulus below 200 °C in BNT-based relaxors can be best-explained by assuming a diffuse ferroelastic phase transition of PNRs.[7] In order to quantify the interval width where most changes in Y occur, tangents are constructed for the initial linear region, the intermediate linear region, and the final saturated region. The intersection of the former two yields $T_{onset,1}$, a measure for the temperature of the minimum Young's modulus. The intersection of the latter two tangents provides $T_{onset,2}$, which affords an estimation of the onset of saturation. Both values are listed for all investigated materials in Table I. BNT-20BKT has a $T_{onset,1}$ of 98 ± 5 °C and a $T_{onset,2}$ of 493 ± 5 °C. The addition of 4 mol. % BZT causes a shift of both temperatures to $T_{onset,1} = 96 \pm 5$ °C and $T_{onset,2} = 535 \pm 5$ °C. It must be noted that Feile *et al.*[48] found a correlation between the minimum in Y(T) and the freezing temperature of single crystals of the solid solution $(KBr)_{1-x}(KCN)_x$, a dipole glass system. In the presently investigated lead-free systems, by contrast, the minimum in Y(T) is largely invariant on composition while freezing shifts to notably lower temperatures. The interval ΔT between both onset temperatures is broad at 395 ± 5 °C for BNT-20BKT and 439 ± 5 °C for BNT-20BKT-4BZT. This general progression is also in good agreement with the relaxor PMN as measured by ultrasound[49] and Brillouin light scattering,[50] where Young's modulus (C_{11}) was found to vary likewise across hundreds of degrees centigrade.

TABLE I. Onset-temperatures T_{onset1} and T_{onset2}, temperature interval of transition ΔT, room temperature Young's modulus $Y_{25\,°C}$, and maximum relative deviation ΔY from room temperature Young's modulus. Note that all temperatures are estimated to have a maximum error of ±5 °C.

Composition	T_{onset1}/ °C	T_{onset2}/ °C	ΔT/ °C	$Y_{25\,°C}$/GPa	ΔY/%
BNT-19BKT-0BZT	98	493	395	100	11.9
BNT-19BKT-4BZT	96	535	439	112	9.8
BNT-6BT	114	488	374	103	12.1
BNT-6BT-2KNN	90	509	419	111	11.2
PZT	228	295	67	66	54.2
PLZT	68	216	148	99	29.2

It is noted that the onset of the saturation behavior is near the Curie point T_C of PZT and Burns temperature T_B of PLZT, both of which are located near ~300 °C. By analogy, it is suggested that T_B of the studied BNT-based relaxors can be estimated from the onset of the saturation behavior at ~700 °C, consistent with the previous studies.[7,51] Consequently, it is suggested that measuring $Y(T)$ up to 900 °C or 1000 °C and comparing with dielectric and TEM measurements could be useful in verifying if T_B can be determined from elastic measurements. Such a high-temperature approach, however, is not trivial and is thus reserved for future investigations.

Another important observation is the increase in room temperature stiffness with incorporation of BZT, which can be rationalized by two potential mechanisms. First, the stiffening may be induced by the chemical modification with the heterovalent zinc ions. Similar effects are well-known for metals, where solid solution hardening is employed to increase strength and hardness but also the Young's modulus.[52] The effect of solid solution hardening is also known for both structural[53] and functional ceramics, for example, iron doping of PZT increases the elastic stiffness.[54]

Second, the BZT modification increases the volume fraction of the metrically cubic phase at the expense of the non-cubically distorted PNRs. The high-temperature cubic phase of PZT[21] and PLZT,[25] in addition to other perovskites such as ST[42] or BT,[19] displays a higher Young's modulus than the respective low-temperature phases of lower symmetry. Judging from unit cell parameters reported for BT, the FE-PE transition is not coupled to an increase in unit cell size.[55] Therefore, the higher Y of the cubic phase is not caused by a higher packing density but is probably related to the higher symmetry. Accordingly, an increase in volume fraction of the pseudocubic phase may cause an increase in Young's modulus. As stated in Table I, the effect of enhanced Young's modulus by chemical modification is observed also for the BNT-6BT-100yKNN system, where 2 mol. % KNN increase Y from 103 GPa to 111 GPa. It is apparent from Figs. 1 and 2 that the modified compositions display higher elastic moduli throughout the whole temperature range.

V. CONCLUSIONS

In conclusion, measurement of the resonance frequency afforded a detection of changes in the local structure caused by the thermal evolution of PNRs. These structural changes are not evidenced in high-resolution X-ray diffraction due to the small length scale of the effect. It was suggested that a minimum in the temperature-dependent Young's modulus should be the result of a diffuse ferroelastic phase transition. In addition, it was found that the modification with a ternary end-member resulted in an increases in the Young's modulus.

ACKNOWLEDGMENTS

This work was financially supported by the Deutsche Forschungsgemeinschaft (DFG) under SFB595/A1. Use of the Advanced Photon Source, an Office of Science User Facility operated for the U.S. Department of Energy (DOE) Office of Science by Argonne National Laboratory, was supported by the U.S. DOE under Contract No. DE-AC02-06CH11357. We would like to acknowledge Dr. Matthew Suchomel for technical assistance and useful discussion. K.G.W. acknowledges support by the Deutsche Forschungsgemeinschaft under WE 4972/1-1. J.L.J. acknowledges the U.S. Department of the Army under W911NF-09-1-0435 for enabling his contributions.

[1]G. A. Smolenskii, V. A. Isupov, A. I. Agranovskaya, and N. N. Krainik, Sov. Phys. Solid State **2**, 2651 (1961).
[2]B. Jaffe, R. S. Roth, and S. Marzullo, J. Appl. Phys. **25**, 809 (1954).
[3]J. Rödel, W. Jo, K. T. P. Seifert, E. M. Anton, T. Granzow, and D. Damjanovic, J. Am. Ceram. Soc. **92**, 1153 (2009).
[4]J. E. Daniels, W. Jo, J. Rödel, and J. L. Jones, Appl. Phys. Lett. **95**, 032904 (2009).
[5]R. Dittmer, W. Jo, J. Daniels, S. Schaab, and J. Rödel, J. Am. Ceram. Soc. **94**, 4283 (2011).
[6]S. Said and J. P. Mercurio, J. Eur. Ceram. Soc. **21**, 1333 (2001).
[7]W. Jo, S. Schaab, E. Sapper, L. A. Schmitt, H.-J. Kleebe, A. J. Bell, and J. Rödel, J. Appl. Phys. **110**, 074106 (2011).
[8]S. T. Zhang, A. B. Kounga, E. Aulbach, H. Ehrenberg, and J. Rödel, Appl. Phys. Lett. **91**, 112906 (2007).
[9]F. Wang, M. Xu, Y. Tang, T. Wang, W. Shi, and C. M. Leung, J. Am. Ceram. Soc. **95**, 1955 (2012).
[10]A. Ullah, C. W. Ahn, A. Hussain, S. Y. Lee, H. J. Lee, and I. W. Kim, Curr. Appl. Phys. **10**, 1174 (2010).
[11]E. A. Patterson, D. P. Cann, J. Pokorny, and I. M. Reaney, J. Appl. Phys. **111**, 094105 (2012).
[12]W. Jo, T. Granzow, E. Aulbach, J. Rödel, and D. Damjanovic, J. Appl. Phys. **105**, 094102 (2009).
[13]W. Jo, R. Dittmer, M. Acosta, J. Zang, C. Groh, E. Sapper, K. Wang, and J. Rödel, J. Electroceram. **29**, 71 (2012).
[14]R. Dittmer, E.-M. Anton, W. Jo, H. Simons, J. E. Daniels, M. Hoffman, J. Pokorny, I. M. Reaney, and J. Rödel, J. Am. Ceram. Soc. **95**, 3519 (2012).
[15]E. Aksel, J. S. Forrester, J. L. Jones, P. A. Thomas, K. Page, and M. R. Suchomel, Appl. Phys. Lett. **98**, 152901 (2011).
[16]R. Dittmer, W. Jo, D. Damjanovic, and J. Rödel, J. Appl. Phys. **109**, 034107 (2011).
[17]A. A. Bokov and Z. G. Ye, J. Mater. Sci. **41**, 31 (2006).
[18]G. A. Samara, J. Phys. Condes. Matter **15**, R367 (2003).
[19]B. L. Cheng, M. Gabbay, G. Fantozzi, and W. Duffy, Jr., J. Alloys Compd. **211–212**, 352 (1994).
[20]E. M. Bourim, H. Tanaka, M. Gabbay, G. Fantozzi, and B. L. Cheng, J. Appl. Phys. **91**, 6662 (2002).
[21]E. M. Bourim, H. Idrissi, B. L. Cheng, M. Gabbay, and G. Fantozzi, J. Phys. IV **6**, 633 (1996).
[22]Y. N. Huang, Y. N. Wang, and H. M. Shen, Phys. Rev. B **46**, 3290 (1992).
[23]A. Bouzid, E. M. Bourim, M. Gabbay, and G. Fantozzi, J. Eur. Ceram. Soc. **25**, 3213 (2005).
[24]D. Viehland, S. J. Jang, E. Cross, and M. Wuttig, Philos. Mag. A **64**, 835 (1991).
[25]D. Viehland, S. J. Jang, L. E. Cross, and M. Wuttig, J. Appl. Phys. **69**, 6595 (1991).
[26]F. Cordero, F. Craciun, F. Trequattrini, E. Mercadelli, and C. Galassi, Phys. Rev. B **81**, 144124 (2010).
[27]X.-C. Zheng, G.-P. Zheng, Z. Lin, and Z.-Y. Jiang, Ceram. Int. **39**, 1233 (2013).
[28]ASTM E1876, "Standard Test Method for Dynamic Young's Modulus, Shear Modulus, and Poisson's Ratio by Impulse Excitation of Vibration," ed. (West Conshohocken, PA: ASTM International, 2009).
[29]W. Jo, C. Park, and D.-Y. Kim, Acta Cryst. A **63**, 229 (2007).
[30]P. Bonneau, P. Garnier, G. Calvarin, E. Husson, J. R. Gavarri, A. W. Hewat, and A. Morell, J. Solid State Chem. **91**, 350 (1991).
[31]Z. G. Lu, C. Flicoteaux, and G. Calvarin, Mater. Res. Bull. **31**, 445 (1996).
[32]Y. Yao, Y. Yang, S. Ren, C. Zhou, L. Li, and X. Ren, Europhys. Lett. **100**, 17004 (2012).
[33]J. Hao, W. Bai, W. Li, B. Shen, and J. Zhai, J. Mater. Res. **27**, 2943 (2012).
[34]E.-M. Anton, L. A. Schmitt, M. Hinterstein, J. Trodahl, B. Kowalski, W. Jo, H.-J. Kleebe, J. Rödel, and J. L. Jones, J. Mater. Res. **27**, 2466 (2012).
[35]R. L. Coble and W. D. Kingery, J. Am. Ceram. Soc. **39**, 377 (1956).
[36]J. B. Wachtman and D. G. Lam, J. Am. Ceram. Soc. **42**, 254 (1959).
[37]D. R. Askeland and P. P. Fulay, *Essentials of Materials Science and Engineering* (Cengage Learning, Toronto, 2009).
[38]J. B. Wachtman, Jr., W. E. Tefft, D. G. Lam, Jr., and C. S. Apstein, Phys. Rev. **122**, 1754 (1961).
[39]E. J. Huibregtse, W. H. Bessey, and M. E. Drougard, J. Appl. Phys. **30**, 899 (1959).
[40]A. -M. M. Baker and J. Mead, in *Handbook of Plastics, Elastomers, and Composites*, 4th ed., edited by C. A. Harper (McGraw-Hill Professional, New York City, 2002).
[41]I. Štubňa, A. Trník, F. Chmelík, and L. Vozár, in *Advances in Ceramics-Characterization, Raw Materials, Processing, Properties, Degradation and Healing*, edited by C. Sikalidis (InTech, 2011).
[42]A. V. Kityk, W. Schranz, P. Sondergeld, D. Havlik, E. K. H. Salje, and J. F. Scott, Europhys. Lett. **50**, 41 (2000).
[43]M. Alguero, B. Jimenez, and L. Pardo, Appl. Phys. Lett. **83**, 2641 (2003).
[44]E. R. Leite, A. M. Scotch, A. Khan, T. Li, H. M. Chan, M. P. Harmer, S.-F. Liu, and S.-E. Park, J. Am. Ceram. Soc. **85**, 3018 (2002).
[45]P. S. Silva, Jr., O. Florêncio, E. R. Botero, J. A. Eiras, and D. Garcia, Mater. Sci. Eng. A **521–522**, 224 (2009).
[46]X. Dai, A. DiGiovanni, and D. Viehland, *Dielectric Properties of Tetragonal Lanthanum Modified Lead Zirconate Titanate Ceramics* (AIP, 1993), p. 3399.
[47]A. Kholkin, A. Morozovska, D. Kiselev, I. Bdikin, B. Rodriguez, P. P. Wu, A. Bokov, Z. G. Ye, B. Dkhil, L. Q. Chen, M. Kosec, and S. V. Kalinin, Adv. Funct. Mater. **21**, 1977 (2011).
[48]R. Feile, A. Loidl, and K. Knorr, Phys. Rev. B **26**, 6875 (1982).
[49]S. N. Dorogovtsev and N. K. Yushin, Ferroelectrics **112**, 27 (1990).
[50]S. G. Lushnikov, A. I. Fedoseev, S. N. Gvasaliya, and S. Kojima, Phys. Rev. B **77**, 104122 (2008).
[51]J. Kling, W. Jo, R. Dittmer, S. Schaab, and H.-J. Kleebe, J. Am. Ceram. Soc. **96**, 3312 (2013).
[52]R. Labusch, Phys. Status Solidi B **41**, 659 (1970).
[53]R. C. Bradt, J. Am. Ceram. Soc. **50**, 54 (1967).
[54]R. Herbiet, H. Tenbrock, and G. Arlt, Ferroelectrics **76**, 319 (1987).
[55]H. F. Kay and P. Vousden, Philos. Mag. **40**, 1019 (1949).